J. Appl. Comput. Mech., 8(4) (2022) 1315-1323
DOI: 10.22055/jacm.2022.39944.3492

ISSN: 2383-4536
jacm.scu.ac.ir

Shahid Chamran University of Ahvaz

Journal of Applied and Computational Mechanics

Research Paper

Influence of Up-down-up Constitutive Equation Parameters on Yield Plateau Stage of Mild Steel Samples Subjected to Stretching

Artyom O. Chirkov[1], Mikhail O. Eremin[2]

[1] National Research Tomsk State University, 36 Lenin Pr., Tomsk, 634050, Russian Federation, Email: chirkovartyem@gmail.com

[2] Institute of Strength Physics and Materials Science of the Siberian Branch of the Russian Academy of Sciences, 2/4 Akademicheskii Pr., Tomsk, 634055, Russian Federation, Email: eremin@ispms.ru

Received February 03 2022; Revised March 03 2022; Accepted for publication March 17 2022.
Corresponding author: M.O. Eremin (eremin@ispms.ru)

Abstract. In this work, the computational study of Lüders phenomenon is addressed. The material for investigation is low-carbon steel demonstrating the yield point phenomenon when pulled in tension. Modeling of samples loading is carried out in the framework of three-dimensional finite-difference method. Judging by the literature review, there is a lack of papers thoroughly addressing the curves of dependences of Lüders elongation and front propagation velocity on parameters of up-down-up constitutive equation. This work fills this gap. It is shown that the difference between the true upper and lower yield stresses, and strain hardening factor have a strong impact on the duration of the yield plateau stage and ratio of front propagation velocity v_f to loading velocity v_l. The results of computational study complement the experimental data presented in available literature.

Keywords: Numerical modeling, Lüders bands, von Mises criterion, fronts, finite-difference analysis, up-down-up equation.

1. Introduction

Phenomenon of discontinuous yielding was first observed in the 19th century [1]. Since that time, pronounced phenomenon attracted much attention and was studied in numerous papers, both experimental and theoretical [1-4]. When loading laboratory dog bone samples of some mild steels, transition from elastic to plastic state is frequently manifested as a switching wave from elastic to plastic state. This process is initiated by a stress drop in the loading curve when effective nucleus of Lüders band is formed. This phenomenon was named after Lüders, who was one of the first to observe it in tensile testing [1]. Related to the macroscopic $\sigma - \varepsilon$ curve, nucleation of bands of localized plastic deformation occurs upon reaching the observed upper yield point and followed by relatively constant stress at observed lower yield point [1,5] (see Fig. 1 for stress-strain curve of a mild steel in initial stages of plastic flow).

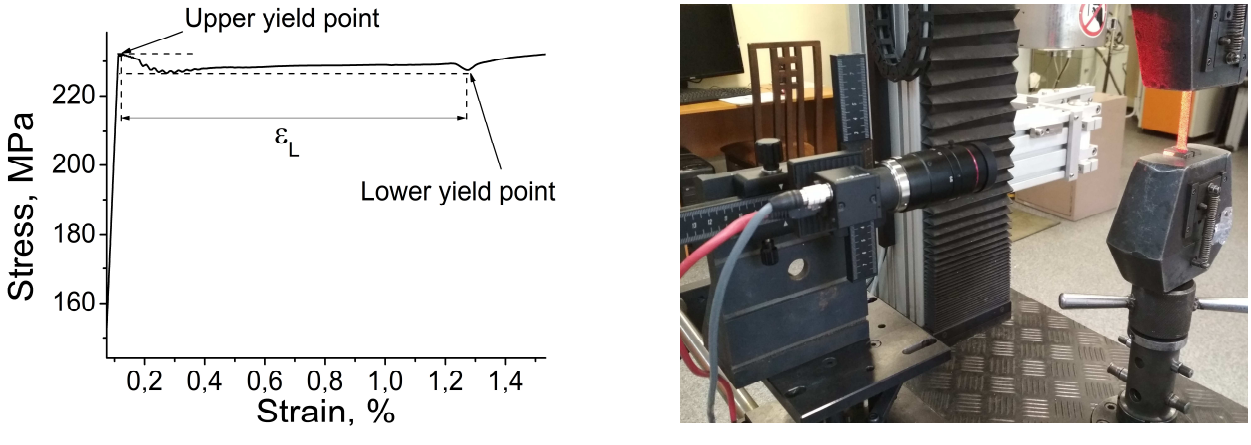

Fig. 1. Stress-strain curve (engineering) of a mild steel sample pulled in tension in elastic and yield plateau stages of plastic flow (by courtesy of Zuev L.B.) (a), experimental setup (b).

Published online: March 28 2022

Transition to a plastic state in the form of Lüders band can be interpreted as a local loss of stability attributed to the relaxation and recovery of stress behind the front. Investigation of different types of plastic flow instabilities is acute problem of modern physics and solid mechanics since it allows for developing the methods to suppress undesirable non-homogeneous distributions of strains. The problem importance is also due to the fact that the instabilities of the deformation process make a significant contribution to the formation of critical states in loaded solids [6].

Recent works focused on the macroscopic effects of Lüders phenomenon and used the continuum mechanics approach [1-3, 5, 7-9]. Several mathematical models of Lüders banding have been proposed to describe numerically the nucleation and propagation of localized plastic deformation bands in low carbon steels, aluminum alloys, etc., [1-3, 10]. A three-dimensional microstructure-based model [3] was developed to reproduce a gradual change in the grain size in the transition region between the heat-affected zone and base material low-carbon steel. A double-limit yield criterion was used to describe Lüders band propagation. It was found that several kinds of interfaces are responsible for different degrees of stress concentration. A Lüders front is one of them. An elastic-viscous-plastic model describing static strain ageing was proposed in [10]. The model was used to simulate the Lüders band propagation in a low-carbon ferritic steel under simple tension and simple shear. It has been noticed that the von Mises plasticity criterion cannot be used in the model to simulate properly both tensile and shear for anisotropic rolled sheets. Instead, the Hosford equivalent stress measure was employed which allows for more realistic simulation. Gradient-enhanced formulations were used to simulate Lüders band propagation in shape memory alloy NiTi by one-dimensional model of pseudoelasticity with micromorphic-type regularization [11]. The incremental energy minimization framework combined with the augmented Lagrangian treatment of the resulting non-smooth minimization problem was used. A thermomechanically coupled model was implemented into finite-element code. The model predicts the effect of the loading rate on the localization pattern and agrees fairly well with experimental data.

Almost all mathematical models of Lüders banding are based on the so-called “up-down-up” constitutive equation which was apparently first used to simulate Lüders banding in [12]. Its schematic representation is given in Fig. 2. The physical reasons for such a form of loading in a point of continuum is that nucleation of plastic flow demands higher stress level rather than maintenance of its development [3]. Underlying physical mechanisms associated with dislocation motion and local stress relaxation are discussed comprehensively in [13].

Despite an extensive previous research, there is a lack of papers thoroughly addressing the dependence of Lüders elongation, bands propagation velocity on the parameters of “up-down-up” constitutive equation. In this work, we try to fill the gap and perform a comprehensive numerical study of the “up-down-up” constitutive equation parameters effect on the Lüders response of loaded samples. In a contrast to complex mathematical models using the microparameters to describe the instability of plastic flow (pinning and/or multiplication of dislocations) we use purely phenomenological approach for simplicity. The novelty of the present study lies in the establishment of regularities in the change in the propagation velocities of Lüders fronts and the Lüders elongation on the magnitude and duration of the stress relaxation and recovery.

Numerical study of the yield point phenomenon has certain advantages and sufficiently complement the experimental data. It is due to the following reasons: (i) true upper yield stress is masked due to unavoidable stress concentrations in experiment, but in the model, it represents a parameter with a certain value assigned; (ii) the rate of work hardening at the front of Lüders band is unmeasurable parameter in experiment, but also enters the model with certain assigned value.

2. Materials and Methods

The models of samples with a gage part measured 50×10×2 mm and the physical-mechanical properties of a mild steel are designed for this study (see Fig. 3 for schematic representation of samples geometry). For the sake of modeling simplicity, we consider only the gage part of sample. The material is assumed to be isotropic.

Modeling of samples loading is carried out in the framework of three-dimensional finite-difference method. It is based on the explicit time integration scheme of solid mechanics dynamic equations. Some details of the numerical method are discussed in Appendix A. However, for exhaustive discussion of the numerical method applied the reader is referred to elsewhere [14]. Numerical modeling was carried out using the model presented below and implemented into available original solver written in Fortran. Calculations were made using multicore workstation on the basis of AMD Threadripper 2950 16-core processor.

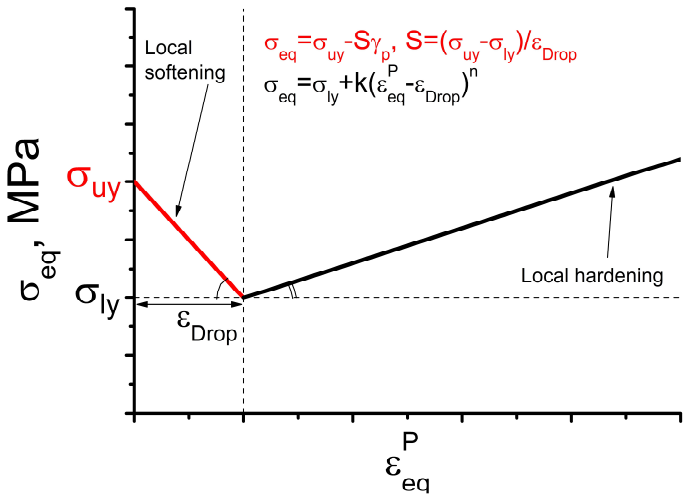

Fig. 2. Schematic representation of “up-down-up” constitutive equation in a point of continuum. An example of linear hardening law is taken when hardening exponent n is equal to unity.

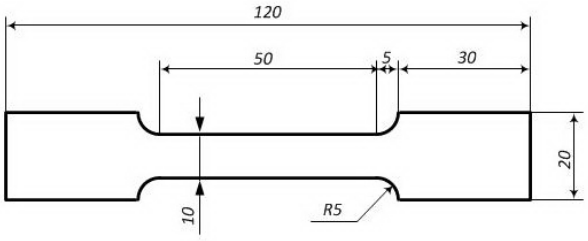

Fig. 3. Schematic representation of the dog bone sample pulled in tension.

3. Mathematical Formulation of Boundary Value Problem

3.1 Governing equations and elastic constitutive response

The basis of the mathematical model is the system of solid mechanics equations [3, 14-18]. The governing equations are the laws of mass (Eq. 1) and momentum (Eq. 2) conservation. The system also contains geometric relations for the total strain rate (Eq. 3) and vorticity (Eq. 4) tensors.

$$\rho V = \rho_0 V_0 \tag{1}$$

$$\rho \dot{v}_i = \frac{\partial \sigma_{ij}}{\partial x_j} \tag{2}$$

$$2\dot{\varepsilon}_{ij} = \frac{\partial v_i}{\partial x_j} + \frac{\partial v_j}{\partial x_i} \tag{3}$$

$$2\dot{\omega}_{ij} = \frac{\partial v_i}{\partial x_j} - \frac{\partial v_j}{\partial x_i} \tag{4}$$

wherein ρ_0, ρ, V_0, V are the initial and current values of density and volume, respectively, v_i is the velocity vector components, σ_{ij} is the Cauchy stress tensor components, x_i is the Cartesian coordinates.

The relations of a hypo-elastic isotropic continuum are used as constitutive equations. In the framework of isotropic medium assumption, there are only two constants in equation of state, namely the bulk (K) and shear (μ) moduli. Their values could be transferred directly from the experiments. The stress tensor is decomposed into volumetric (Eq. 5) and deviatoric (Eq. 6) parts:

$$\dot{P} = -K\dot{\theta}^T \quad , \quad \dot{\theta}^T = \dot{\varepsilon}_{ii}^T \tag{5}$$

$$\dot{S}_{ij} + S_{ik}\dot{\omega}_{ik} - S_{kj}\dot{\omega}_{ik} = 2\mu\left(\dot{\varepsilon}_{ij}^T - \frac{1}{3}\dot{\theta}^T\delta_{ij} - \dot{\varepsilon}_{ij}^P\right) \tag{6}$$

wherein P is an isotropic pressure, θ is a volumetric strain, S_{ij} is the deviatoric stress tensor, ε_{ij}^p is the plastic strain tensor, dot above the symbols designates the time derivative.

The Jaumann corotation derivative in Eq. 6 is applied to subtract the rotation of the cell (particle or element of a medium) as a whole which does not contribute to the values of deviatoric stresses.

The constitutive equations describing the plastic strains demand some discussion. Note, that we state the independence of the elastic continuum response on plastic flow. In that case, the total strain rate is divided into two parts (Eq. 7), wherein indices T, E and P correspond to total, elastic and plastic strain rates, respectively:

$$\dot{\varepsilon}_{ij}^T = \dot{\varepsilon}_{ij}^E + \dot{\varepsilon}_{ij}^P \tag{7}$$

3.2 Plastic flow

As a part of constitutive response, the von Mises yield criterion (Eq. 8) is employed which is widely accepted for metals [3, 13, 15].

$$f\left(\sigma_{ij}, \varepsilon_{eq}^P\right) = \tau - Y \tag{8}$$

wherein $f(\sigma_{ij})$ is the yield function, ε_{eq}^p is the equivalent plastic strain, $\tau = \sqrt{\frac{1}{2}S_{ij}S_{ij}}$ is the second invariant of deviatoric stress tensor, Y is the current yield strength. Taking into account the "up-down-up" constitutive equation, current yield strength of a single continuum point is described by piece-wise function (Eq. 9, see Fig. 2) [19]:

$$Y = \begin{cases} \sigma_{Uy} - \dfrac{\Delta\sigma}{\varepsilon_{Drop}}\varepsilon_{eq}^P & ,\text{if } 0 < \varepsilon_{eq}^P \le \varepsilon_{Drop} \\ \sigma_{Ly} + k\left(\varepsilon_{eq}^P - \varepsilon_{Drop}\right) & ,\text{if } \varepsilon_{eq}^P > \varepsilon_{Drop} \end{cases} \tag{9}$$

wherein σ_{Uy} is the upper yield stress, σ_{Ly} is the lower yield stress, $\Delta\sigma$ is the difference between upper and lower yield stresses, ε_{Drop} is the value of equivalent plastic strain limiting width of a drop stage, k is the strain hardening factor. Thus, nucleation of plastic flow occurs when the upper yield stress is reached. The stress relaxation takes place next, and only after reaching the value of the lower yield stress, local work hardening is pronounced.

Table 1. The physical-mechanical properties and value ranges of the model parameters.

ρ, g/cm^3	K, GPa	G, GPa	σ_{Uy}, MPa	$\Delta\sigma$, MPa	k, MPa	ε_{Drop}
7.846	172	79.2	165	1-40	200-300	0.01-0.03

The results below represent a parametric study wherein only three parameters of the model – namely, strain-hardening factor k, difference between the upper and lower yield points $\Delta\sigma$ and plastic strain limiting drop stage ε_{Drop} were varied at other parameters being equal. The range of the "up-down-up" constitutive equation parameters is given in Table 1 as well as values of some material constants – density and elastic moduli.

3.3 Boundary and initial conditions

The following boundary conditions were applied to the model:
(i) the nodal v_z velocity component was assigned to the nodes belonging to the opposite Z-plane edges – $v_z = v(t)$ and $v_z = -v(t)$, respectively;
(ii) the free-of-stress surface condition is maintained at all other facets of the sample;
(iii) the restriction of nodes sliding is made by v_x and v_y components of the velocity vector being zero.
An initial state of the sample corresponds to zero values of all stress-strain parameters.
The technique of a very slow loading was used, when determining the function $v(t)$, to minimize the dynamic effect. Notably, the time of the loading increase corresponds to approximately 10 runs of elastic P-wave through the entire computational domain which yields the quasi-static condition of stress-strain evolution and minimizes the influence of an acceleration term in Eq. 2.

4. Results of Modeling and Discussion

4.1 Numerical convergence

For the sake of simplicity, we used a local criterion of plasticity (see Eq. 8). The local criteria are widely known to produce the computational mesh sensitivity and spurious strain localizations (e.g. [20]). Therefore, one of the first major step of any computer modeling is to verify the convergence of a numerical solution. The number of mesh elements (voxels in the case of regular finite-difference mesh) is increased in the computational domain until a reasonable trade-off between the accuracy and computational costs is reached. Here, we verified the convergence of the numerical solution based on the von Mises stress value averaged in the whole computational domain. Its dependence on the number of mesh elements is provided in Fig. 4. The numerical data (black quads) are approximated by exponential function. Notably, that the dependence is a nonlinear curve reaching the asymptotic value of exponential function when the number of mesh elements is ≈4 million. It can be seen that complete convergence is not reached. However, further increase in the number of mesh elements is rather costly and does not make a significant contribution to the numerical solution convergence. Therefore, the mesh with ≈7.5 million elements was chosen as a reasonable trade-off and is used in further analysis.

4.2 Origination and propagation of Lüders band

Figure 5a illustrates an obtained stress-strain curve of computer model in initial stages of deformation – namely, the elastic and initial stages of plastic flow. For clarity, the instants (a) – (d) in the curve are matched with the corresponding patterns of plastic strain rate. Upon reaching the upper yield point (state (a) in Fig. 5a) two symmetric bands of strain localization in the form of cross originate near the sample supports and start to propagate towards each other. In a contrast to experimental studies wherein inclined single band generally originates near one of the supports, the numerical solution gives the strain localization in the form of cross. The latter is the result of idealized conditions of computational study when both conjugate directions of maximum tangential stress have an equal influence.

Formation of effective nuclei of Lüders bands is accompanied by the stress drop straight after the elastic part of the loading curve. Judging by the obtained numerical results, the same patterns (symmetric bands) are observed in all performed modeling with different values of k, ε_{Drop} and $\Delta\sigma$. Bands of strain localization are inclined to the loading direction at angles of ≈ 54-58 degrees.

The loading diagram of considered example suggests that propagation of Lüders bands occurs at relatively constant observed lower yield stress $\sigma \approx 225$ MPa. The values of k, ε_{Drop} and $\Delta\sigma$ for this particular case are provided in Fig. 5 caption. The patterns of plastic strain rate for the other states (b) – (d) are illustrated in Fig. 5b.

Once the Lüders bands have travelled across the entire sample and switched the material from elastic to plastic state, the linear strain hardening onset is pronounced. Discussion of this stage of plastic flow falls out of this article scope and is disregarded.

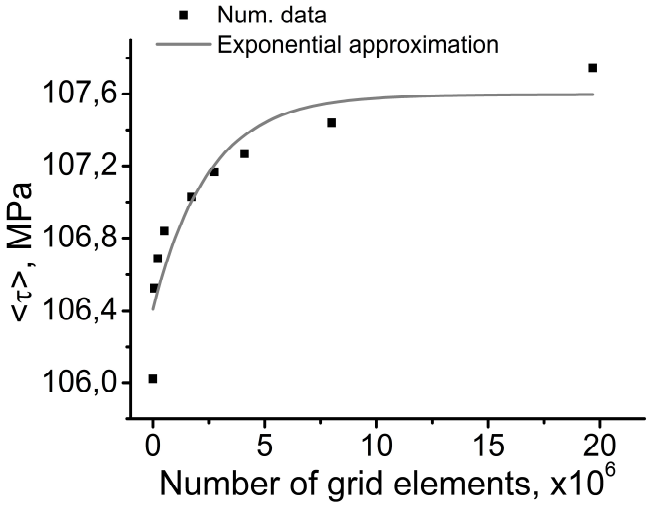

Fig. 4. Numerical solution mesh sensitivity test result.

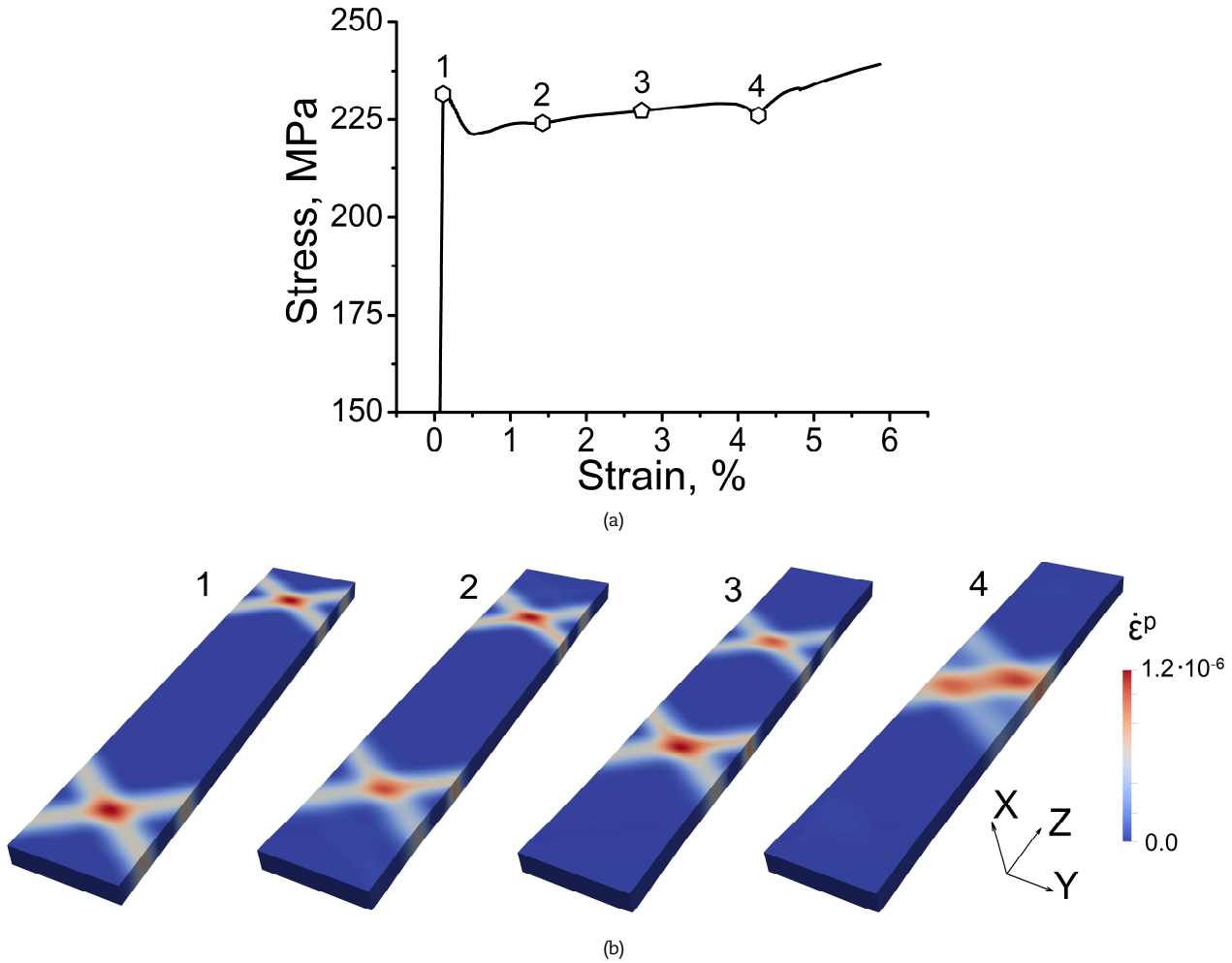

Fig. 5. Stress-strain curve in the yield plateau stage for $\Delta\sigma$=10MPa, ε_{Drop}=0.03 and strain hardening factor k=200MPa with marked instants a–d (a), the patterns of equivalent plastic strain rate ($\dot{\varepsilon}^p$) in consecutive instants (a–d) of Lüders bands propagation (b).

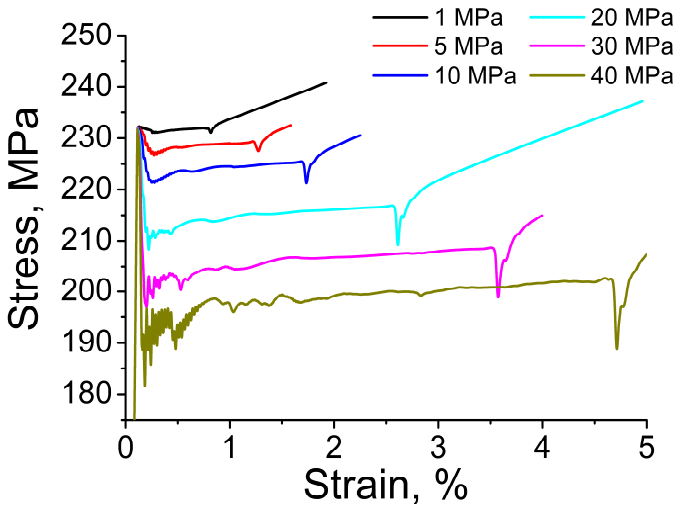

Fig. 6. Stress-strain curves in the yield plateau stage for different $\Delta\sigma$ and strain hardening factor k=300 MPa, ε_{Drop}=0.01.

4.3 v_f/v_l ratio and Lüders elongation curves of dependence on model parameters

According to Eq. 9 the von Mises stress in a point of continuum reaches the σ_{Uy} first. First yielding of material results in accumulation of plastic strain. The latter in its turn results first in local strain softening and further strain hardening. It is clear that deformation process will be concentrated in just yielded part of sample because current local yield strength is lower here than in other parts of sample. Once the strain hardening recovers the local yield strength of material to the stress amount at some distance ahead of the front, namely the observed lower yield stress, the Lüders band might further propagate. This process is exhaustively discussed in [1] based on the analytical solution. Here, we analyze the results of numerical modeling to obtain some curves of dependence related to stress drop, drop strain and strain hardening factor.

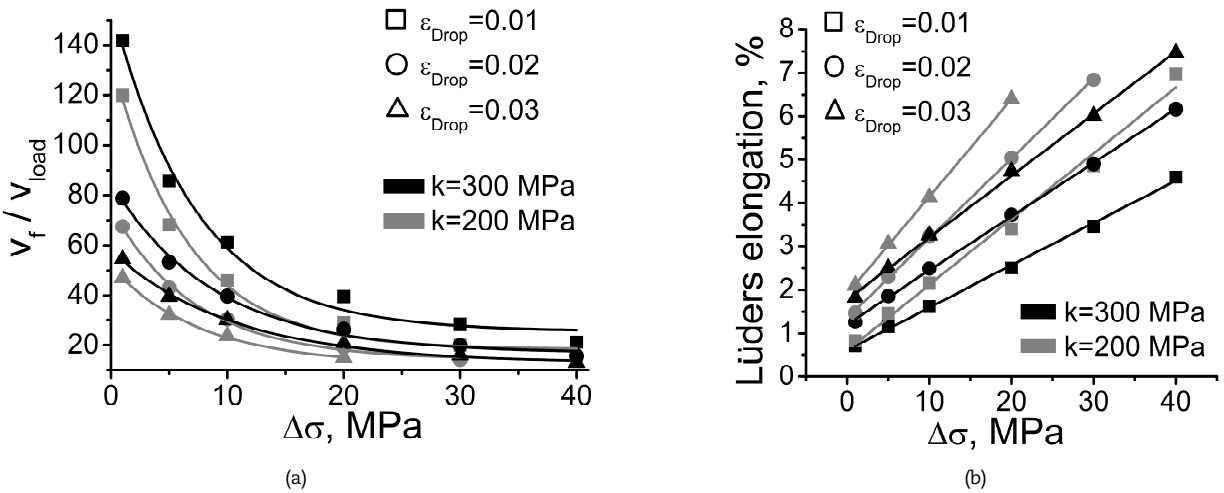

(a) (b)

Fig. 7. Curves of v_f/v_l ratio dependence on $\Delta\sigma$ (a), curves of the Lüders elongation dependence on $\Delta\sigma$ (b) for different values of k and ε_{Drop}.

The curves in Fig. 6 illustrate as an example the yield plateau stage for different values of $\Delta\sigma$ and fixed value of k=100MPa and ε_{Drop} = 0.01. It can be noted that the higher the $\Delta\sigma$ the higher the macroscopic stress drop and the longer the yield plateau stage in macroscopic loading diagram. Analogous modeling was carried out for the whole considered range of k and ε_{Drop} values (see Table 1).

The results of parametric study of Lüders band v_f/v_l ratios and Lüders elongation are illustrated in Fig. 7. The ratios v_f/v_l for different $\Delta\sigma$, k and ε_{Drop} are illustrated in Fig. 7a. It can be noted that for low values of $\Delta\sigma$ (not exceeding 5 MPa) and sharp drop ($\varepsilon_{Drop} \leq 0.01$) from the true upper yield stress to the lower one, the v_f/v_l exceeds 100. It indicates that the switching wave of plastic deformation travels across the entire sample with quite high velocity. Apparently, the limit velocity of considered plastic wave is the Kolsky plastic waves propagating with speed proportional to the square root of work hardening factor. With further increase in $\Delta\sigma$ a noticeable change in v_f/v_l ratio occurs and becomes close to that observed in experimental studies, e.g. [4, 21]. Obtained ratios also satisfy the rule-of-thumb $\sum v_f/v_l \approx 1/\varepsilon_L$ proposed in pioneer work of Dr. J. Butler [22].

A set of dependence curves of Lüders elongation on $\Delta\sigma$ are close to linear, increasing functions (Fig. 7b). It can be noted that the Lüders elongation increases with increasing of ε_{Drop} and decreasing of hardening factor k at fixed value of $\Delta\sigma$. In other words, the more the local drop in shear strength occurs, the longer the strength will be recovered due to strain hardening.

5. Conclusion

In this work, uniaxial tension of mild steel sample was studied by the means of three-dimensional finite-difference analysis. As a part of constitutive response, the up-down-up equation coupled with J_2-plasticity was employed for the purpose of work. Parameters of the model were discretely changed to obtain the curves of dependence of several macroscopic regularities of the yield point phenomena – namely, the Lüders elongation, and ratio of the front velocity to loading velocity. Obtained results are in good agreement with both experimental findings, e.g. [4, 23, 24] and analytical and numerical studies [1, 19]. Despite the reasonably good simulation of Lüders banding might be performed using "up-down-up" constitutive equation, yet it represents a static equation of state, i.e. the strain-rate sensitivity of materials could not be described by single set of varied parameters. This fact is a major limitation of considered model, which is apparently applicable in the case of low strain rates applied, when material demonstrates insufficient strain rate sensitivity.

In a future work, we plan to analyze comprehensively an influence of the sample geometry on the Lüders performance of mild steels using up-down-up constitutive equation and use the elasto-viscous-plastic models to simulate the strain rate sensitivity of mild steels

6. Appendix A

Figure A1 provides a supplementary material for determination of the Lüders band velocity and inclination angle. The Lüders band velocity is determined as the ratio between the positions x2 and x1 and the time interval Δt. The inclination angle is determined as the localization band slope angle with respect to the tensile direction.

6.1 Some details of numerical method

The numerical scheme of the second order of accuracy is explicit and, thus, is conditionally stable. The latter means that there is a restriction on the time integration step under the Courant condition (A.1).

$$\Delta t^n \leq c\frac{\Delta x^n}{v_p}, \tag{A.1}$$

wherein n is the number of integration cycle, c is the Courant ratio (typically equal to one third), Δx^n is the lowest characteristic length among all elements (voxels), determined as the ratio between the voxel volume and the largest area of one of the six voxel sides, and v_p is the sound velocity of a P-wave.

The partial derivatives within the method applied are replaced by the finite-difference analogue on the basis of the following equations. An expression is written for the partial derivative of an arbitrary function P by X, other directions (Y and Z) follow the same logic. The partial derivative represents the flux through the surface S which bounds the control volume V (Eq. A.2). The difference in the flux in and out of the control volume is the result of induced change in the quantity of an arbitrary function P:

$$\frac{\partial P}{\partial X} = \lim_{V\to 0}\int_{(S)}\frac{P(n,i)dS}{V}, \tag{A.2}$$

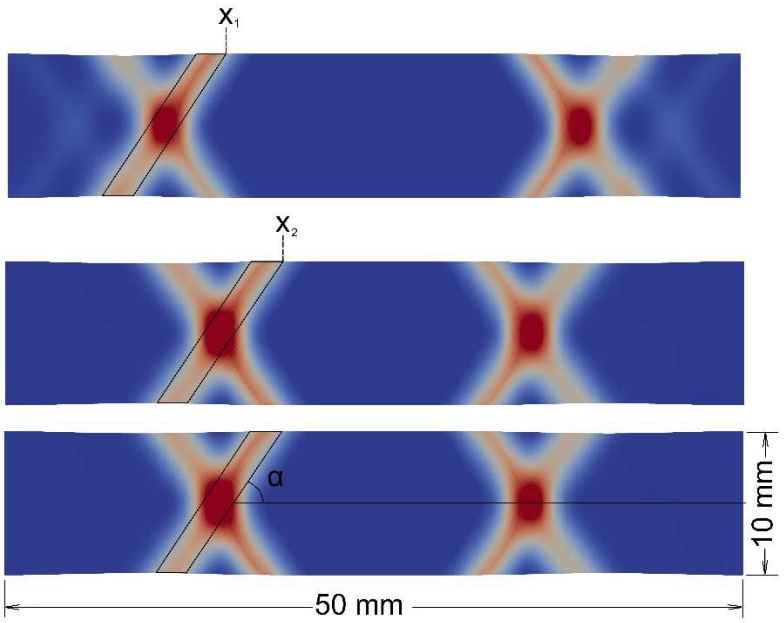

Fig. A1. Illustration to the determination of the Lüders front velocity and inclination angle.

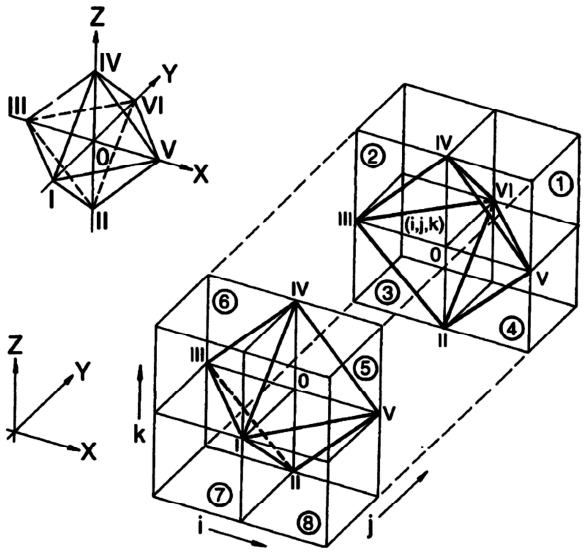

Fig. A2. Template for integration of equations of motion, i, j, k = Lagrange coordinates.

wherein n and i are the outward normal to the surface, and the X unit vector, dS is an element of surface area.

Based on the template for integration of equations of motion (Fig. A2), the node i,j,k is surrounded by eight cells marked with figures $1-8$. The stress gradient between these cells yields a non-zero acceleration of the node i,j,k. Equation A.3 is the momentum conservation law along the Ox direction, Eq. A.4 represents the finite-difference analogue of the Σ_{xx} stress tensor component gradient with respect to the Eq. A.2. Finite-difference analogues for T_{xy} and T_{xz} are formed in the same manner with the necessary replacements of components and coordinates. The other two equations of motion are solved in the same way to obtain the accelerations in the Oy and Oz directions.

Once the accelerations are determined, the nodal velocities at $n+1/2$ are calculated by Eq. A.5, and nodal coordinates at $n+1$ and $n+1/2$ are calculated by Eq. A.6 and A.7, respectively.

$$\left(\frac{d\dot{x}}{dt}\right)^n_{i,j,k} = \frac{1}{\rho^n_{i,j,k}}\left[\frac{\partial \Sigma_{xx}}{\partial x} + \frac{\partial T_{xy}}{\partial y} + \frac{\partial T_{xz}}{\partial z}\right]^n_{i,j,k} \tag{A.3}$$

$$\begin{aligned}\frac{1}{\rho^n_{i,j,k}}\left(\frac{\partial \Sigma_{xx}}{\partial x}\right)^n_{i,j,k} = \frac{1}{4\Phi_{i,j,k}}\Big(&(\Sigma_{xx})_1[(y_{VI}-y_V)(z_{IV}-z_V)-(Z_{VI}-Z_V)(Y_{IV}-Y_V)]+(\Sigma_{xx})_4[(y_{II}-y_V)(z_{VI}-z_V)-(z_{II}-z_V)(y_{VI}-y_V)]\\ &+(\Sigma_{xx})_2[(y_{IV}-y_{III})(z_{VI}-z_{III})-(z_{IV}-z_{III})(y_{VI}-y_{III})]+(\Sigma_{xx})_3[(y_{VI}-y_{III})(z_{II}-z_{III})-(z_{VI}-z_{III})(y_{II}-y_{III})]\\ &+(\Sigma_{xx})_5[(y_V-y_I)(z_{IV}-z_I)-(z_V-z_I)(y_{IV}-y_I)]+(\Sigma_{xx})_8[(y_{II}-y_I)(z_V-z_I)-(z_{II}-z_I)(y_V-y_I)]\\ &+(\Sigma_{xx})_7[(y_I-y_{III})(z_{IV}-z_{III})-(z_I-z_{III})(y_{IV}-y_{III})]+(\Sigma_{xx})_6[(y_{II}-y_{III})(z_I-z_{III})-(z_{II}-z_{III})(y_I-y_{III})]\Big)^n_{i,j,k}\end{aligned} \tag{A.4}$$

$$\dot{x}^{n+1/2}_{i,j,k} = \dot{x}^{n-1/2}_{i,j,k} + (\frac{d\dot{x}}{dt})^{n}_{i,j,k}\Delta t^{n} \tag{A.5}$$

$$x^{n+1}_{i,j,k} = x^{n}_{i,j,k} + \dot{x}^{n+1/2}_{i,j,k}\Delta t^{n+1/2} \tag{A.6}$$

$$x^{n+1/2}_{i,j,k} = x^{n}_{i,j,k} + \frac{1}{2}\dot{x}^{n+1/2}_{i,j,k}\Delta t^{n+1/2} \tag{A.7}$$

The complete system of solid mechanics equations is solved using an original software written by Dr. Eremin in Fortran.

Author Contributions

Sections 1, 2 were performed by M.O. Eremin. The rest work was performed by A.O. Chirkov.

Acknowledgments

The authors expressed gratitude to the anonymous reviewer and editors of the journal whose critical comments allowed to improve the quality of article.

Conflict of Interest

The authors declared no potential conflicts of interest concerning the research, authorship, and publication of this article.

Funding

The work of M.O. Eremin was made according to the Government research assignment for ISPMS SB RAS, project FWRW-2021-0002. The work of A.O. Chirkov was supported by the Russian Foundation for Basic Research, grant 20-31-90016.

Data Availability Statements

The datasets generated and/or analyzed during the current study are available from the corresponding author on reasonable request.

References

[1] Schwab, R., Ruff, V., On the nature of the yield point phenomenon, *Acta Materialia*, 61(5), 2013, 1798-1808.
[2] Hallai, J., Kyriakides, S., On the effect of Luders bands on the bending of steel tubes. part II: Analysis, *International Journal of Solids and Structures*, 48(24), 2011, 3285-3298.
[3] Romanova, V., Balokhonov, R., Schmauder, S., Three-dimensional analysis of mesoscale deformation phenomena in welded low-carbon steel, *Materials Science and Engineering: A*, 528(15), 2011, 5271-5277.
[4] Danilov, V., Gorbatenko, V., Zuev, L., Orlova, D., Kinetics and morphology of Luders deformation in specimens with homogeneous structure and with a weld joint, *Materials Science and Engineering: A*, 714, 2018, 160-166.
[5] Johnson, D., Edwards, M., Chard-Tuckey, P., Microstructural effects on the magnitude of Luders strains in a low alloy steel, *Materials Science and Engineering: A*, 625, 2015, 36 – 45.
[6] Makarov, P., Eremin, M., Jerky flow model as a basis for research in deformation instabilities, *Physical Mesomechanics*, 17(1), 2014, 62-80.
[7] Wenman, M., Chard-Tuckey, P., Modelling and experimental characterisation of the Luders strain in complex loaded ferritic steel compact tension specimens, *International Journal of Plasticity*, 26(7), 2010, 1013-1028.
[8] Coer, J., Manach, P., Laurent, H., Oliveira, M., Menezes, L., Piobert-Luders plateau and Portevin-le Chatelier effect in an Al-Mg alloy in simple shear, *Mechanics Research Communications*, 48, 2013, 1-7.
[9] Mao, B., Liao, Y., Modeling of Luders elongation and work hardening behaviors of ferrite-pearlite dual phase steels under tension, *Mechanics of Materials*, 129, 2019, 222-229.
[10] Maziere, M., Luis, C., Marais, A., Forest, S., Gasperini, M., Experimental and numerical analysis of the Luders phenomenon in simple shear, *International Journal of Solids and Structures*, 106-107, 2017, 305-314.
[11] Hajidehi, M., Stupkiewicz, S., Gradient-enhanced model and its micromorphic regularization for simulation of Lüders-like bands in shape memory alloys, *International Journal of Solid and Structures*, 135, 2018, 208-218.
[12] Shaw, J.A., Kyriakides, S., Initiation and propagation of localized deformation in elasto-plastic strips under uniaxial tension, *International Journal of Plasticity*, 13(10), 1997, 837-871.
[13] Hall, E.O., *Yield Point Phenomena in Metals and Alloys*, Springer Science & Business Media, 1970.
[14] Wilkins, M., Computer Simulation of Dynamic Phenomena, Springer-Verlag., 1999
[15] Makarov, P.V., Smolin, I.Yu., Khon, Yu.A., Eremin, M.O., Bakeev, R.A., Peryshkin, A.Yu., Zimina, V.A., Chirkov, A., Kazakbaeva, A.A., and Akhmetov, A.Zh., Autosoliton View of the Seismic Process. Part 2. Possibility of Generation and Propagation of Slow Deformation Autosoliton Disturbances in Geomedia, *Physical Mesomechanics*, 24(4), 2021, 375–390.
[16] Balokhonov, R., Zinoviev, A., Romanova, V., Zinovieva, O., The computational micromechanics of materials with porous ceramic coatings, *Meccanica*, 51(2), 2016, 415-428.
[17] Smolin, I., Makarov, P., Eremin, M., Matyko, K., Numerical simulation of mesomechanical behavior of porous brittle materials, *Procedia Structural Integrity*, 2, 2016, 3353-3360.
[18] Eremin, M.O., Chirkov, A.O., Nadezhkin, M.V., Zuev, L.B., Microstructure-based finite-difference analysis of the plastic flow in low-carbon steel, *European Journal of Mechanics - A/Solids*, 93, 2022, 104531.
[19] Makarov, P.V., Smolin, I.Yu., Zimina, V.A., The structure of deformation autosoliton fronts in rocks and geomedia, *Geodynamics & Tectonophysics*, 12(1), 2021, 100-111.
[20] Lim, H., Battaile, C.C., Bishop, J.E., Foulk, J.W., Investigating mesh sensitivity and polycrystalline RVEs in crystal plasticity finite element simulations, *International Journal of Plasticity*, 121, 2019, 101-115.
[21] Barannikova, S., Ponomareva, A.V., Zuev, L.B., Vekilov, Yu.Kh., Abrikosov, I.A., Significant correlation between macroscopic and microscopic parameters for the description of localized plastic flow auto-waves in deforming alloys, *Solid State Communications*, 152(9), 2012, 784-787.
[22] Butler, J.F., Lüders front propagation in low carbon steels, *Journal of the Mechanics and Physics of Solids*, 10(4), 1962, 313–318.
[23] Danilov, V., Gorbatenko, V., Zuev, L., Orlova, D., Danilova, L., Luders deformation of low-carbon steel, *Steel in Translation*, 47(10), 2017, 662-668.
[24] Zuev, L., Barannikova, S., Experimental study of plastic flow macro-scale localization process: Pattern, propagation rate, dispersion, *International Journal of Mechanical Sciences*, 88, 2014, 1-7.

ORCID iD

Artyom O. Chirkov https://orcid.org/0000-0002-6152-8023
Mikhail O. Eremin https://orcid.org/0000-0002-5740-8221

How to cite this article: Chirkov A.O., Eremin M.O. Influence of Up-down-up Constitutive Equation Parameters on Yield Plateau Stage of Mild Steel Samples Subjected to Stretching, *J. Appl. Comput. Mech.*, 8(4), 2022, 1315–1323. https://doi.org/10.22055/jacm.2022.39944.3492